Nonlinear Dyn (2008) 52: 181–197
DOI 10.1007/s11071-007-9270-x

ORIGINAL PAPER

Parametric identification of a chaotic base-excited double pendulum experiment

Yang Liang · B.F. Feeny

Received: 18 July 2006 / Accepted: 5 April 2007 / Published online: 6 June 2007

Abstract The parametric identification of a chaotic system was investigated for a double pendulum. From recorded experimental response data, the unstable periodic orbits (UPOs) were extracted and then used in a harmonic balance identification process. By applying digital filtering, digital differentiation and linear regression techniques for optimization, the results were improved. Verification of the related simulation system and linearized system also corroborated the success of the identification algorithm.

Keywords Parametric identification · Harmonic balance · Chaotic system · Unstable periodic orbits · Double pendulum

1 Introduction

Parametric identification is important for the construction of mathematical models of vibration systems. Until now, most of the methods of parametric identification of nonlinear systems have focused on free vibration, random excitation or periodically forced steady state vibration behavior [1–8]. Kapania [4] used finite element analysis for identification of dynamic systems with the assumption of weak nonlinearity. In [5], Volterra series and higher order frequency response functions (FRF) were used for parameter estimation of non-chaotic nonlinear systems. Gottlieb [6] and Feldman [7] investigated the identification of single- and two-degree-of-freedom systems by means of the Hilbert transform. In [1], nonlinear resonances by random excitations were utilized, some of the parameters were identified. Meanwhile, since damping and friction were found hard to estimate, many researchers [2, 3, 8] investigated methods of identifying those parameters, many of which are time domain methods.

Recently, the application of chaotic behavior in parametric identification has begun to be noticed and some related algorithms were developed. In [9], the Poincaré section and limit cycles were used for system identification. Meanwhile, a fundamental property of deterministic chaos is that the chaotic set of a dynamical system contains an infinite number of unstable periodic orbits. Furthermore, multiple approximated periodic orbits can be extracted from a phase space reconstruction [10–13], and can be applied for identification purposes, which is an important advantage over a one-periodic-orbit steady state system, since more periodic orbits can usually provide more information about a nonlinear system. The unstable periodic orbits make the identification in the chaotic world much simpler. Many methods previously used for non-chaotic

Y. Liang (✉) · B.F. Feeny
Department of Mechanical Engineering, Michigan State University, East Lansing, MI 48824, USA
e-mail: yang.liang@schaeffler.com

B.F. Feeny
e-mail: feeny@egr.msu.edu

systems can be applied to chaotic systems with knowledge of UPOs. Yasuda et al. [14, 15] introduced an inverse applied harmonic-balance method to estimate parameters. Plakhtienko [16, 17] also introduced a method of a special weight function, by which the second order differential equation could be converted to a series of linear equations if some periodic orbits can be known a priori. In [16], it is noticeable that if harmonic functions are applied as weighting functions, the rest of the procedure is identical to the harmonic balance method. Ghanem [18] investigated the wavelet-based method for system identification. Both the wavelet and harmonic balance methods can be applied to the identification of chaotic systems. The harmonic balance method is more feasible for systems with time-invariant parameters. Based on the harmonic method, Feeny and Yuan [19] developed a general method for chaotic systems that extracts unstable periodic orbits and then exploits the harmonic balance method to predict the parameters. Furthermore, they [20] applied this technique to an experimental magneto-elastic oscillator; results were accurate and also noise-resistant. The present study is based upon their algorithm. But unlike all of these applications, which are single-degree-of-freedom systems, the purpose of this report is to apply and examine the algorithm on a multi-degree-of-freedom system with strong nonlinearity.

The work discussed in this report is a further investigation and application of harmonic balance to parametric excited chaotic systems [19]. It includes a simulation verification [21] and an experimental study, which will be introduced in this part of the report.

The experimental work involves a double pendulum system with parametric excitation that is strongly nonlinear. Since this double pendulum is a multi-degree-of-freedom one, many new issues showed up in the experiment. Also, some modifications were applied to the identification process in order to extend the theory to the strongly nonlinear, multi-degree of freedom system. Modifications included digital differentiation and other techniques of error reduction.

In the following parts of the paper, the system configuration and equations of motion will be described and derived. The method and improvements that were used in the identification will be described. Then, the experimental apparatus and configuration will also be explained. In the last two parts of the report, results will be presented and discussed, and several conclusions will be drawn.

2 Description of the double pendulum system

A schematic diagram of the double pendulum is shown in Fig. 1. The first arm (central arm) has mass m_1, centroid offset e_1, arm length l_1, and angular inertia J_{c1} based upon the arm centroid point. The second arm (small arm) has mass m_2, centroid offset e_2, arm length l_2, and angular inertia J_{c2}. θ_1 is the absolute angular displacement of the first arm and θ_2 is the relative angular displacement of the second arm. The pin O undergoes a vertical sinusoidal imposed displacement $y(t)$.

The two arms of the pendulum are supported and connected by low friction bearings. The bearings are assumed to have two types of friction: dry Coulomb friction and viscous damping. In the specific double pendulum that was used in the experiment, isolated free vibration tests indicated that the first arm bearings had dominantly Coulomb friction because of no oil lubrication, and the second arm bearings had dominantly viscous friction due to full oil lubrication. With these known properties, we can then obtain the non-dimensional governing differential equations of this system:

$$\begin{cases} \ddot{\phi}_1 + b_{11}\ddot{\phi}_2 \cos(\phi_2 - \phi_1) - b_{11}\dot{\phi}_2^2 \sin(\phi_2 - \phi_1) \\ \quad + b_{12}\sin\phi_1 + b_{13}\sin\phi_1 \ddot{y} + c_{11} f(\dot{\phi}_1) \\ \quad - c_{12}(\dot{\phi}_2 - \dot{\phi}_1) = 0, \\ \ddot{\phi}_2 + b_{21}\ddot{\phi}_1 \cos(\phi_2 - \phi_1) + b_{21}\dot{\phi}_1^2 \sin(\phi_2 - \phi_1) \\ \quad + b_{22}\sin\phi_2 + b_{23}\sin\phi_2 \ddot{y} \\ \quad + c_2(\dot{\phi}_2 - \dot{\phi}_1) = 0, \end{cases} \tag{1}$$

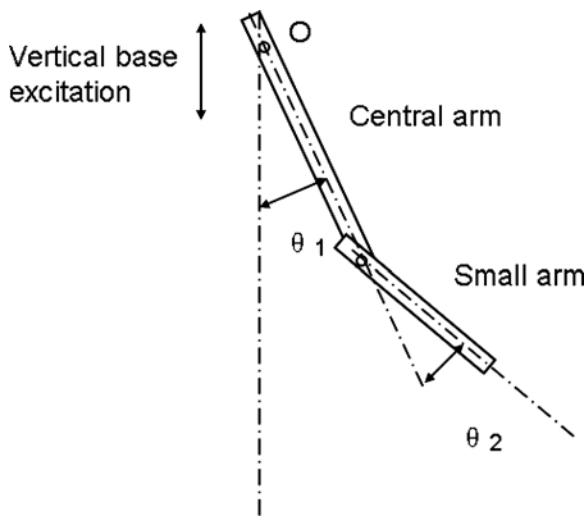

Fig. 1 A sketch of the double pendulum

where $\phi_1 = \theta_1$ and $\phi_2 = \theta_1 + \theta_2$ are absolute angular deflections, $b_{11} = \frac{m_2 e_2 l_1}{J_{o1}}$, $b_{12} = \frac{g(m_1 e_1 + m_2 l_1)}{J_{o1}}$, $b_{13} = \frac{(m_1 e_1 + m_2 l_1)}{J_{o1}}$, $b_{21} = \frac{m_2 e_2 l_1}{J_{o2}}$, $b_{22} = \frac{g m_2 e_2}{J_{o2}}$, $b_{23} = \frac{m_2 e_2}{J_{o2}}$, $c_{12} = \frac{c_{r2}}{J_{o1}}$, $c_2 = \frac{c_{r2}}{J_{o2}}$, $J_{o1} = J_{c1} + m_1 e_1^2 + m_2 l_1^2$, and $J_{o2} = J_{c2} + m_2 e_2^2$; y is the excitation displacement of the support with known frequency f_e; and

$$f(x) = \text{sign}(x) = \begin{cases} 1, & x > 0, \\ 0, & x = 0, \\ -1, & x < 0 \end{cases}$$

is a sign function representing Coulomb friction. Function $f(x)$ is valid if there are no sticks. For convenience of the analysis, a nondimensional form of the governing differential equation is desired. By letting $\tau = 2\pi f_e t$ and $\Omega = 2\pi f_e$, then, $\frac{d}{dt} = \frac{d}{d\tau} \cdot \frac{d\tau}{dt} = 2\pi f_e \frac{d}{d\tau} = \Omega \frac{d}{d\tau}$. Under a sinusoidal excitation $y = E_1 \cos\tau + F_1 \sin\tau$, $a = \sqrt{E_1^2 + F_1^2}$, where a is the excitation amplitude, (1) can be expressed as

$$\begin{cases} B_{11}\phi_2'' \cos(\phi_2 - \phi_1) - B_{11}\phi_2'^2 \sin(\phi_2 - \phi_1) \\ \quad + B_{12}\sin\phi_1 + B'_{13}\sin\phi_1 \cos\tau \\ \quad + B'_{14}\sin\phi_1 \sin\tau + C_{11} f(\phi_1') \\ \quad - C_{12}(\phi_2' - \phi_1') = -\phi_1'', \\ B_{21}\phi_1'' \cos(\phi_2 - \phi_1) + B_{21}\phi_1'^2 \sin(\phi_2 - \phi_1) \\ \quad + B_{22}\sin\phi_2 + B'_{23}\sin\phi_2 \cos\tau \\ \quad + B'_{24}\sin\phi_1 \sin\tau + C_2(\phi_2' - \phi_1') = -\phi_2'', \end{cases} \tag{2}$$

where $\phi_i' = \frac{d\phi_i}{d\tau}$, $B_{i1} = b_{i1}$, $B_{i2} = b_{i2}/\Omega^2$, $B_{i3} = -b_{i3}E_1$, $B_{i4} = -b_{i3}F_1$, $C_{11} = c_{11}/\Omega^2$, $C_{12} = c_{12}/\Omega$, $C_2 = c_2/\omega$, for i=1, 2. Equation (2) is then the desired form for identification.

3 Method

The identification process is similar to the one used in the simulation system of the parametrically excited single pendulum [21], which contains data acquisition/post-processing, phase plane reconstruction/extracting unstable periodic orbits, formation of the identification matrix and the solution by the least mean square method. Some signal noise occurred during digitization. Therefore certain digital filtering techniques were applied to the acquired signals. Other modifications are also applied to the double pendulum system for improved identification.

Due to the complexity of the nonlinearity of the double pendulum equation (2), our unknown parameters contain only those coefficients of terms of the differential equations which will greatly simplify the identification matrix. There are totally 11 unknown parameters in the two differential equations, namely, B_{11}, B_{12}, …, B_{24}, C_{11}, C_{12} and C_2. Similar to the case in [21], the angular displacement θ_1 and θ_2 are variables in S^1 (one-dimensional sphere space). However, the angular velocities, accelerations and $\sin\phi_i$ ($i = 1, 2$) belong to R^1 (one-dimensional continuous real space). Hence, for any period k orbit (there may be multiple orbits of same periodicity k, the Fourier series expressions are

$$\phi_{1,k,l}(t) \approx \Omega_{1,k,l}t + \frac{a_{0,k,l}}{2} + \sum_{j=1}^{m}\left(a_{j,k,l}\cos\frac{j\omega t}{k} + b_{j,k,l}\sin\frac{j\omega t}{k}\right) \tag{3}$$

and

$$\phi_{2,k,l}(t) \approx \Omega_{2,k,l}t + \frac{c_{0,k,l}}{2} + \sum_{j=1}^{m}\left(c_{j,k,l}\cos\frac{j\omega t}{k} + d_{j,k,l}\sin\frac{j\omega t}{k}\right), \tag{4}$$

where $\Omega_{i,k,l}$, is the average rotation speed per cycle for the lth orbit of period k. Thus,

$$\dot{\phi}_{1,k,l}(t) \approx \Omega_{1,k,l} + \sum_{j=1}^{m}\frac{j\omega}{k}\left(-a_{j,k,l}\cos\frac{j\omega t}{k} + b_{j,k,l}\sin\frac{j\omega t}{k}\right), \tag{5}$$

$$\dot{\phi}_{2,k,l}(t) \approx \Omega_{2,k,l} + \sum_{j=1}^{m}\frac{j\omega}{k}\left(-c_{j,k,l}\cos\frac{j\omega t}{k} + d_{j,k,l}\sin\frac{j\omega t}{k}\right), \tag{6}$$

where $k = 1, 2, \ldots, K$, is the corresponding period of the orbit; K is the maximum periodicity. Likewise, the Fourier series of other terms in the equation can be expressed. Meanwhile, for the nondimensional differential equations, time t here is actually τ in equation (2), and the fundamental frequency is 1. If incremental encoders are used to sense the angular displacements, then the velocity and acceleration

are not directly measured. But, their Fourier transformations can be handily generated by using the Fourier transformation of the displacement. However, for noise-contaminated displacement signals, noisy errors may be amplified in the obtained Fourier spectrum of velocity and acceleration. Also, Fourier series expansions of some terms in the differential equations, such as $\dot{\phi}_{i,k}^2 \sin(\phi_{2,k} - \phi_{1,k})$, are not obtained by direct Fourier series expansion of their time domain signal, but by convolution of known Fourier expansion components with a low-pass filter applied in the frequency domain (see Sect. 5.4). The purpose of applying a low-pass filter to each signal component before convolution is to avoid noise amplification. Substituting (3–6) and the rest of the Fourier series of the nonlinear terms into (2), and equating the coefficients of terms with identical harmonic order, we obtain two matrix equations:

$$A_1 \vec{x}_1 = \vec{q}_1 \tag{7}$$

and

$$A_2 \vec{x}_2 = \vec{q}_2, \tag{8}$$

where $\vec{x}_1$ and $\vec{x}_2$ are vectors of unknown parameters and the rows of A_1 and A_2 are the Fourier coefficients of the corresponding harmonics that multiply the unknown parameters. Given a set of periodic orbits, it is adequate to equate the coefficients of the first several orders of subharmonics since they are usually the major components of the periodic orbits and less contaminated by noise. We then truncate the Fourier series expansion, and take the first M orders, such that $M \cdot K > N_c$, where N_c is the number of unknown coefficients in $\vec{x}_1$ or $\vec{x}_2$. With these conditions satisfied, the two equations can be solved by the least mean square method:

$$\hat{\vec{x}}_1 = \left(A_1^T A_1\right)^{-1} A_1^T \vec{q}_1 \tag{9}$$

and

$$\hat{\vec{x}}_2 = \left(A_2^T A_2\right)^{-1} A_2^T \vec{q}_2. \tag{10}$$

After the nondimensional parameters are identified, the physical properties can then be restored according to the nondimensional parameters' definition if part of the physical parameters can be known prior to identification. In the experiment, m_2, e_2, l_1 were treated as known since these physical properties were easily evaluated.

3.1 Extraction of unstable periodic orbits

We used the reconstructed phase plane to extract unstable periodic orbits (UPO) [11]. Suppose the sampled signal is $s_i(t) = [\theta_i(t)\theta_i(t + T_d)]$ for i=1, 2, and T_d is the time delay for embedding dimensions. An approximated UPO with error tolerance e is extracted if

$$\left\| s_i(t) - s_i(t + kT) \right\| < e_i, \quad i = 1, 2, \tag{11}$$

where T is the excitation period, and k is the periodicity of the recurrence. Then, for example, for a given $k = 4$, if inequality (11) is satisfied, a period 4 orbit is then said to be extracted.

3.2 Uncertainty and error reduction

3.2.1 Friction issues

Previous research [19, 20] indicated that small friction parameters were more difficult to identify accurately than other parameters in experiments for a single degree of freedom system. The inaccuracy can result from several reasons:

1. experimental noise in the sampled data;
2. inadequate sensor sensitivity (the resulting error can also be treated as a noise component);
3. inaccurate model of friction, e.g., viscous friction, dry friction, or their combination;
4. recurrence errors of the extracted UPOs;
5. strong nonlinearity of the investigated system.

Furthermore, if the damping factors are much smaller than other parameters, and the least mean square solution is used, an error deemed small for other parameters can cause relatively large errors for the damping terms.

On the other hand, if the friction coefficients can be determined prior to identification, the identification could likely be improved. In the previous study [20], the friction errors had little influence on other identified parameters in a lightly damped single-degree-of-freedom pendulum system.

3.2.2 Noise contamination in the extracted unstable periodic orbits

In the previous application of the chaotic system identification process [19–21] in which single-degree-of-

freedom systems were examined, the identification algorithm was noise-resistant. However, a similar hypothesis could not be applied to the present two-degree-of-freedom system. The reason is simply due to the strong nonlinearity of the double pendulum, and it can be explained by differences in the governing differential equations.

The governing equation of a horizontally excited single pendulum (examined in [21]) is

$$\ddot{\theta} + c/r\dot{\theta} + 1/r^2 \sin\theta - f \sin t \cos\theta = 0. \tag{12}$$

Although the parametric excitation term is nonlinear, the $\dot{\theta}$ and $\ddot{\theta}$ terms are, on the other hand, linear. The $\sin\theta$ term in (12) can also be regarded as linear in terms of harmonic functions. Suppose the contaminated signal is composed of the real signal and noise $n(t)$: $\theta(t) = \theta_t(t) + n(t)$. The angular velocities and accelerations of the periodic orbits can be obtained by equations similar to (5) and (6). Hence, the noise in the obtained speed and acceleration kth subharmonic is actually amplified by k, though $n(t)$ is rather small in the displacement signal. The overall signals of velocity and acceleration are then considered to be contaminated mainly by high frequency noise. Apparently, to the system (12), where the speed and acceleration terms are all linear, the high frequency noise whose frequency is larger than $(K+1)$th harmonic term will be automatically filtered out, since only the first K terms of harmonic order are used in the identification matrix.This explains why the identification process is noise-resistant for systems like (12).

However, in the double pendulum system (2), the identification process appears to be less noise-resistant than the previous examples since velocities and accelerations do not appear linearly in differential equations. Specifically, it is the $(\phi_i')^2 \sin(\phi_2 - \phi_1)$ and $\phi_i'' \cos(\phi_2 - \phi_1)$ terms that contribute most to the noise inaccuracy of the result. Other high-order terms also have a similar problem of noise amplification. It can be explained by the following FFT equation

$$\mathcal{F}\big[\dot{\phi}_i^2 \sin(\phi_2 - \phi_1)\big] = \mathcal{F}(\dot{\phi}_i)^2 \otimes \mathcal{F}\big[\sin(\phi_2 - \phi_1)\big], \tag{13}$$

where $\mathcal{F}(x)$ represents the Fourier transform of x, and operator $\otimes$ represents convolution. The convolution operation can be expressed by

$$F(\omega) \otimes G(\omega) = \int_{-\infty}^{+\infty} F(\sigma) G(\sigma - \omega) d\sigma, \tag{14}$$

where $F(\sigma)$ and $G(\sigma)$ are two integrable functions. By convolution, the high frequency noise in each component is, therefore, mixed into the final result by convolution since convolution involves the integration of the product between two signals. Furthermore, it actually amplifies the noisy influence of the angular displacement, e.g., high frequency noise, since in the algorithm the frequency components of $\dot{\theta}_i$ and $\ddot{\theta}_i$ are obtained by (5) and (6). Hence, the truncation of the first K harmonic terms could not reduce the disturbance of the noise. Low-pass filters have to be applied to the signals before the convolution to avoid noise convolution.

3.2.3 *Digital differentiation for reduction of the recurrence error*

Recurrence error results from the error tolerance of UPO extraction. It is a major source of noise in the identification process. An impulse caused by differentiation through the recurrence error occurred in the periodic velocity and acceleration curves, which is not true for the real periodic orbits. If we look at the velocity curve, it can be expressed as

$$\dot{\hat{\theta}}(t) = \dot{\theta}(t) + \alpha\delta(t - t_c) + \eta(t), \tag{15}$$

where $\dot{\hat{\theta}}(t)$ is the calculated velocity curve, $\dot{\theta}(t)$ is the real velocity curve, $\alpha\delta(t - t_c)$ is the impulse with amplitude α proportional to the recurrence error, t_c is time delay, and $\eta(t)$ is noise other than the recurrence error, which is considered to be small. Thus, after digital filtering, and applying Fourier transform, we obtain

$$\mathcal{F}(\dot{\theta}) \cong \mathcal{F}(\dot{\hat{\theta}}) + \alpha e^{-jt_c\omega},$$

where α is the expression of the impulse function in frequency domain and is a white noise. Furthermore, this noise contaminates all the subharmonics of the velocity curve, which could not be eliminated by the low-pass digital filter and could hence generate large error in the identification result.

Hence, a five-point differentiation algorithm was applied to obtain the digital derivatives and double derivatives of angular displacements:

$$\begin{aligned}\dot{f}(x) = \big\{&8\big[f(x+h) - f(x-h)\big] \\ &- f(x+2h) + f(x-2h)\big\}[12h]^{-1} \\ &+ o\big(h^4\big)\end{aligned} \tag{16}$$

and

$$\ddot{f}(x) = \{16[f(x+h) + f(x-h) - 2f(x)] - f(x+2h) - f(x-2h) + 2f(x)\}[12h^2]^{-1} + o(h^4). \quad (17)$$

The errors of these algorithms can be reduced with a smaller time interval h. The five-point algorithm can also reduce the influence of high frequency noise.

3.2.4 *Optimized choice of harmonics and subharmonics*

The identification result can vary when a different choice of subharmonics was applied. The problem was not so troublesome in previous applications of the harmonic balance method [19–21] where the nonlinearity was simple and not so strong as the double pendulum case. However, in the present experiment, different subharmonic sets lead to variations in the estimated parameters. It is then necessary for us to seek some general rules for evaluating the result.

In (7) and (8), the choice of the first M subharmonics of each UPO (subharmonics are functions of $\sin(\frac{ix}{k})$ or $\cos(\frac{ix}{k})$ where i and k represents the ith term in Fourier series of a period k orbit) remains an issue. In our pendulum system a periodic orbit whose period is a multiple k of the excitation period, if $M \leq k$, i.e., subharmonic frequencies less than or equal to the driving frequency, would tend to be the best for identification. One reason is that these subharmonics consist of a large part of the displacement signals' energy, and hence contain a relatively small portion of the noise contamination (see Fig. 6). Also, the noise components in the velocity and acceleration signals are reduced according to (5) and (6).

The remaining question is whether it is possible to measure the identification error and use it as an indicator of how 'true' the identification is. To quantify the identification error, we refer to linear regression techniques, borrow some concepts in statistics, and transform (7–10) into

$$\vec{e}_i = A_i \vec{\hat{x}}_i - \vec{q}_i, \quad i = 1, 2, \quad (18)$$

where $\vec{e}_i$ is the residue vector. Then, we can define the identification error ε_i as

$$\varepsilon_i = \frac{\|\vec{e}_i\|_\infty}{\|\vec{\hat{q}}_i\|_\infty},$$

where $\vec{\hat{q}}_i = A_i \vec{\hat{x}}_i$ is the predicted vector of $\vec{q}_i$. With the identification error defined, the rule of thumb for judging a good identification is $\varepsilon_i < \epsilon_c$, where ϵ_c is the positive critical value. $\epsilon_c = 10\%$ was used in the experiment.

Our problem is now how to optimize the identification process so as to improve the accuracy, i.e., minimize the identification error. From the statistics point of view, we have a good linear regression curve if the resulting residues are distributed evenly and randomly around the predicted values. For this purpose, an optimization algorithm was developed to exclude the subharmonic terms which result in large residues, and retain the good terms, which consist of most of the subharmonics and should have small residues. It involves the following steps:

1. Given the set of subharmonics, do the identification process and find out the maximum absolute residue value $e_{\max}$.
2. For a level of significance β, which is a small value, remove from the subharmonics set those subharmonics whose corresponding residue $e > (1-\beta)e_{\max}$.
3. Repeat the first step by using the remaining subharmonics, and compute the identification error ε_i.
4. If $\varepsilon_i < 10\%$, then stop the optimization process and assume that the desired result has been obtained; if not, go back to step 1 with the remaining subharmonics set and repeat the optimization process.

4 Experiment description

Figure 1 shows a sketch of the double pendulum that was used in the experiment. Two optical encoders (US Digital) were separately attached to the central arm (US Digital H5S-1024-157H) and the second arm (US Digital H5S-1024) to measure the relative angular displacements θ_1 and θ_2. Both of the encoders had a resolution of 1024 per cycle, capable of detecting a minimum angular difference of 0.3516°. The two encoders sent out TTL square waves, which are noise-resistant. The TTL signals were then sent to two EDAC (Encoder Digital to Analog Converter) units, which transformed the TTL waves into an analogue signal. After that, a data acquisition terminal translated all the signals into computer-acceptable digital signals.

For validation purposes, Table 1 lists all the physical properties of the double pendulum. The asterisks

Table 1 Physical properties of the double pendulum

m_1 (kg)	0.1362	m_2 (kg)	0.040
e_1 (m)	0.0127	e_2 (m)	0.0267
l_1 (m)	0.0635	l_2 (m)	0.0534
J_1 (kg m^2)*	5.99×10^{-4}	J_2 (kg m^2)*	4.033×10^{-5}
C_{11}*	1.01×10^{-3}	C_1*	0.0485
C_2*	0.00366	–	–

Table 2 Experimental settings

Sampling rate (f_s)	500 Hz	Base freq. (f_e)	5 Hz
Cut-off freq. (f_c)	80 KHz	Amplitude (a)	1.15 cm

in the table denote that some properties are not directly measured, but estimated from other dynamic methods, which implies that those parameters could have small errors. To estimate the mass moment of inertia, a small amplitude free vibration was tested on the double pendulum. By evaluating the two natural frequencies of the system through the FFT, the mass moment of inertia values were calculated. Some parameters related to sampling and experimental setting are listed in Table 2.

With all these settings, the acquired chaotic data was obtained during a 3-hour-long chaotic vibration. The data section lasted 22 minutes.

5 Result band validation

5.1 Phase plane reconstruction & UPO extraction

The embedding dimension was chosen to be eight by the false nearest neighbors method [13]. Mutual information [13] of the signal was used for choosing adequate time delay T_d.

It can be seen from Fig. 2 that there are weak minima of $I(dt)$ at $dt = 5$, 15, 18 and 24. But $T_d = 24$ in a driving period of 100 samples is somewhat close to a quarter period, the ideal delay for a sinusoidal signal. The reconstructed phase portrait is plotted in Fig. 3 with $T_d = 24$. The portrait shows that the central arm represented by θ_1 oscillated in small angles most of the time with occasional large angle whirling, which implies relatively larger noise in θ_1 signal due to the limitation of the optical encoders, whereas, the second arm displacement, represented by θ_2, consisted mainly of whirling vibration.

For the given experimental settings, $f_s = 500$ Hz, $f_e = 5$ Hz, $\mathrm{T} = f_s/f_e = 100$. One data set of 670 000 points was used in analysis. Since there are two angles involved, each with different characteristics, the error tolerance of UPO extraction e was chosen as 5%. For a 5% tolerance, 6 distinct orbits were extracted.

Figure 4 shows an example of the extracted UPOs. We also extracted UPOs up to period 15. In all of the cases, the small arm whirled. In Fig. 4, the central arm whirled, whereas in other cases, the central arm oscillated without whirling.

Compared to [19, 20], the extracted UPOs in this double pendulum system are much fewer than the extracted UPOs in the single-degree-of-freedom systems, which even had tolerance error smaller than 5%. This is because recurrences are less frequent in higher dimensional spaces for small periodicity k. Suppose the number of boxes of size r needed to cover an attractor of dimension α is $N_1 \sim A_1 r^{\alpha}$, where A_1 some constant determined by the chaotic attractor. Roughly assuming evenly distributed data over an chaotic attractor, the probability of recurrently hitting a given box p_1 is $p_1 \sim 1/N_1 \sim 1/A_1 r^{-\alpha}$. Comparing this with another chaotic attractor of dimension β, we have

$$\frac{p_1}{p_2} \sim \frac{A_2}{A_1} r^{\beta-\alpha},$$

which implies that the higher the dimension of a chaotic attractor, the smaller the probability of finding a UPO with tolerance of error r.

5.2 Identified parameters

Table 3 lists all of the identified parameters by Fourier series expansion of UPOs, applying the harmonic balance method with modifications discussed in Sect. 3: low-pass filter, FFT convolution and optimization. The effects of these modifications are examined below. Friction was treated as unknown.

The friction coefficients correspond to negative friction, or to energy generation, which is not physically realistic and therefore deemed inaccurate. However, despite the friction factors inaccuracy, most of other parameters match with the actual values within an error range of 10%, which is generally satisfying for experimental data.

Meanwhile, as we have mentioned before, some of the 'true' values (marked with '*') listed in Table 3 were obtained by indirect dynamical methods, e.g.,

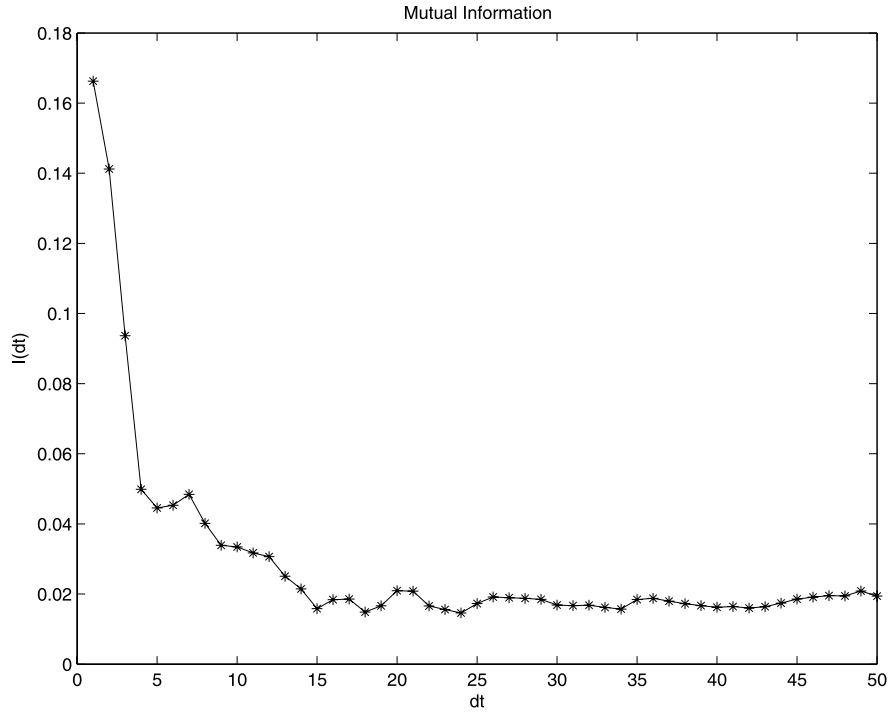

Fig. 2 Mutual information $I(dt)$

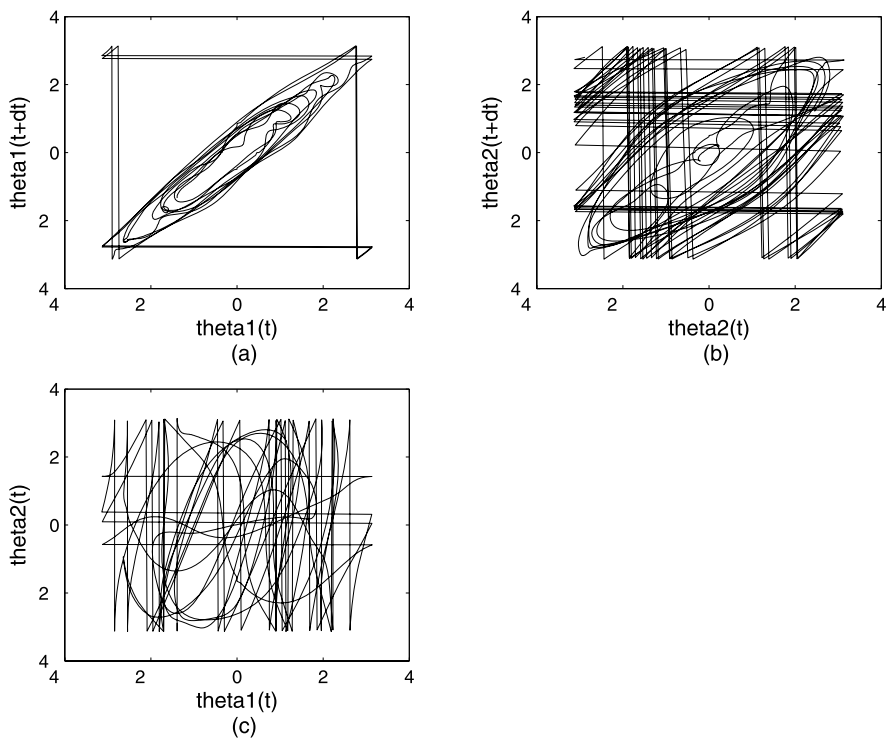

Fig. 3 Phase portrait of experimental data with $dt = 24$, (**a**) $\theta_1(t)$–$\theta_1(t + dt)$, (**b**) $\theta_1(t)$–$\theta_2(t)$, (**c**) $\theta_2(t)$–$\theta_2(t + dt)$; θ is represented by 'theta' in the figure

small angle free vibration, and thus those 'true' physical parameters and related nondimensional parameters may also have some error. Thus, more verification methods were examined (see Sect. 5.6).

Fig. 4 A period 9 UPO

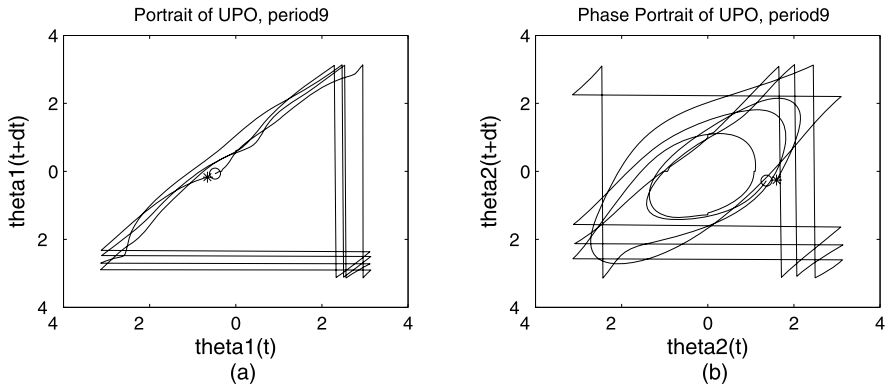

Table 3 Identified parameters by applying low-pass filter, FFT convolution, Fourier series expansion of UPOs, optimization, harmonic balance method with subharmonics whose frequencies are $\leq$ excitation frequency $f_e = 5$ Hz, and subharmonics optimization

	ID values	Settings	Error
B_{11}	0.1167	0.1131	3.2%
B_{12}	0.0781	0.0711	9.8%
B_{13}	0.0809	–	–
B_{14}	0.0264	–	–
$B_{15} = \sqrt{B_{13}^2 + B_{14}^2}$	0.0849	0.0820	3.6%
B_{21}	1.6149	1.6816	4.0%
B_{22}	0.2562	0.2630	3.6%
B_{23}	0.2777	–	–
B_{24}	0.0715	–	–
$B_{25} = \sqrt{B_{23}^2 + B_{24}^2}$	0.2868	0.2913	1.6%
C_{11} *	0.0001	1.02×10^{-3}	–
C_{12} *	0.0007	0.00366	–
C_2 *	0.0106	0.0485	–
J_{o1} (kg m^2)*	5.8113×10^{-4}	5.99×10^{-4}	2.0%
J_{o2} (kg m^2)*	4.1995×10^{-5}	4.033×10^{-5}	3.9%
a (cm)	1.18	1.15	2.6%
$m_1 e_1$ (kg m)	1.73×10^{-3}	1.60×10^{-3}	8.5%

5.3 The friction issue

Our first result has showed that friction coefficients may not be precisely identified due to their small values. The presence of noise decreases the accuracy of the extracted UPOs. Due to reasons mentioned in Sect. 3.2.1, the identified friction coefficients are erroneous, whereas other estimated parameters show only small discrepancies from the real values.

Table 4 Identified nondimensional parameters using low-pass filter, FFT convolution and optimization, provided that the friction coefficients are known

	ID values	True values	Error
B_{11}	0.1178	0.1131	4.2%
B_{12}	0.0774	0.0711	8.8%
B_{13}	0.0829	–	–
B_{14}	0.0185	–	–
$B_{15} = \sqrt{B_{13}^2 + B_{14}^2}$	0.0852	0.0820	3.9%
B_{21}	1.6040	1.6816	4.6%
B_{22}	0.2646	0.2630	0.6%
B_{23}	0.2840	–	–
B_{24}	0.0483	–	–
$B_{25} = \sqrt{B_{23}^2 + B_{24}^2}$	0.2880	0.2913	1.2%

We can assume that the friction parameters are already known, and then identify the other parameters in our harmonic balance method. In this work, we determined the friction in each pendulum bearing by a small amplitude free vibration method. The free vibration test indicated that in the central arm, solely Coulomb friction was involved, and in the second arm, solely viscous friction was involved. The nondimensional form of the friction parameters are listed in Table 1. As such, the friction parameters were estimated by using free vibration decrements. Hence, we applied the identification algorithm with known friction coefficients.

The result in Table 4 shows that the friction parameters, due to their relatively small values (less than 1/5 of other parameters), have little influence on the

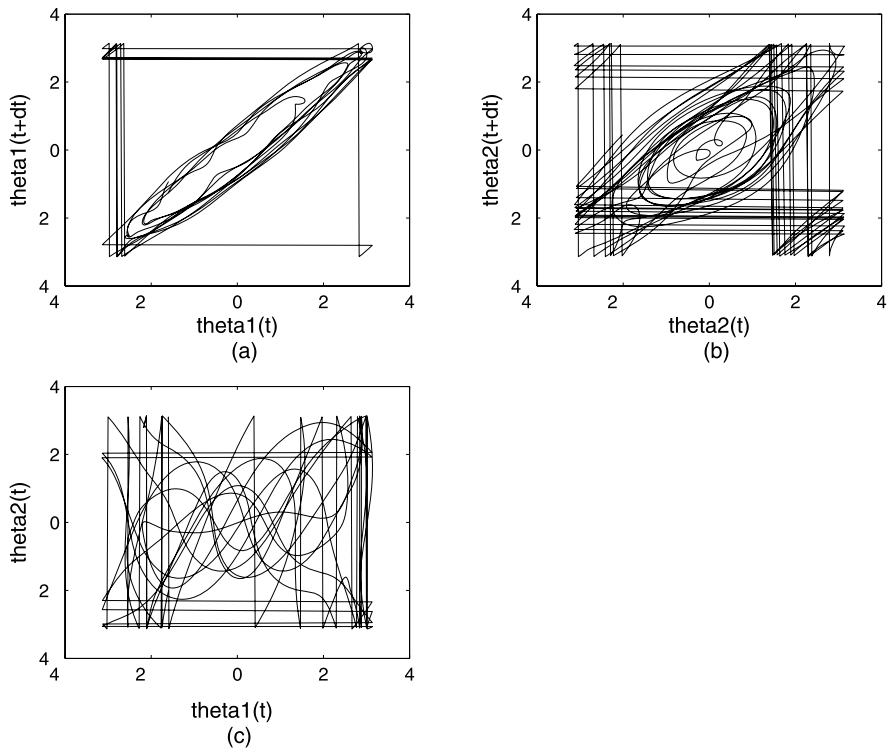

Fig. 5 Phase portrait of the simulated system with $C_{11} = 1.02 \times 10^{-3}$, $C_{11} = 0.0366$ and $C_2 = 0.0485$; $dt = 24$

overall result (the same as happened in [20]). This also implies that the small errors in other parameters can cause a large percent error in the friction terms. Hence, the first result in Table 3 is believed to be reliable for the coefficients of conservative and parametric excitation terms.

For further verification, a simulation of the double pendulum system based on (2) and the identified parameters was examined. However, despite the robustness of the identification process, simulated double pendulum system is extremely sensitive to parameters, e.g., friction coefficients. The simulation was done with Matlab by digital integration. The simulation result was obtained (shown in Fig. 5) with $C_{11} = 1.02 \times 10^{-3}$, $C_{11} = 0.00366$ and $C_2 = 0.0485$ and other parameters set as the identified values in Table 3.

5.4 High frequency noise in unstable periodic orbits

Next we address noise contamination issues of Sect. 3.2.2. One way to avoid noise contamination is to filter out the high frequency noise of the signal after UPO extraction and before convolution. This idea was incorporated in the identification process, and it turned out to be effective. Suppose $y = (\frac{d\phi_i}{d\tau})^2 \sin(\phi_2 - \phi_1)$.

Table 5 Comparison of $\mathcal{F}(y)$ with and without filter added

i	Coefficients of cos (ix)		Coefficients of sin (ix)	
	without filter	with filter	without filter	with filter
1	−3.2486	−0.3087	0.0328	0.0000
2	−34.0713	−27.1330	17.7370	17.7403
3	−15.6946	−8.6732	−23.6908	−23.2652
4	−31.2079	−24.1696	−10.2571	−10.6034

Table 5 compares the difference of the first 4 orders of Fourier series coefficients of y with low pass filtering before convolution and without filtering (shown in Fig. 4). The cut-off frequency was set to be $1/5\,f_s$ Hz. Figure 6 shows the velocity and acceleration frequency spectra of θ_1. It can be seen that the acceleration's high frequency noise is quite intolerable, and even with the low pass filter of $1/5\,f_s$ cut-off frequency, there is still considerable noise remaining.

Displayed in Fig. 7 are also signals with and without the low-pass filter for the period-9 UPO. The low-pass filtered signals are smoother and assumed to be closer to real angular displacements. Meanwhile, an identification process without any filtering was examined by utilizing the same periodic orbits extracted.

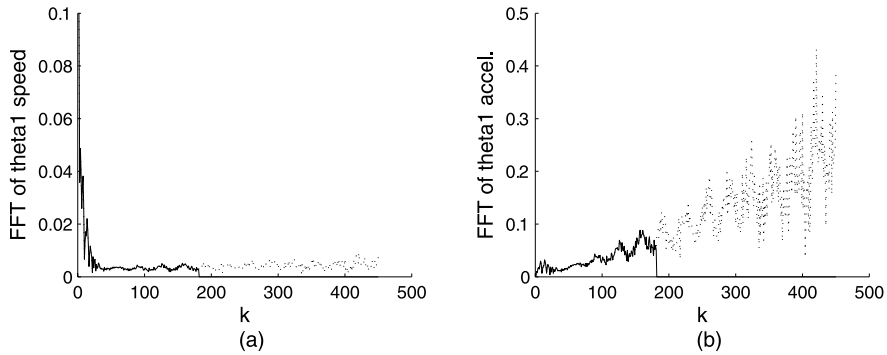

Fig. 6 FFT amplitude of the $\dot{\theta}_1$ and $\ddot{\theta}_1$ with and without low-pass filter applied; the *continuous line* is FFT of signals with filter of $1/5\,f_s$ cut-off frequency; the *dotted line* is FFT of signals without filter; k is the order of Fourier harmonics

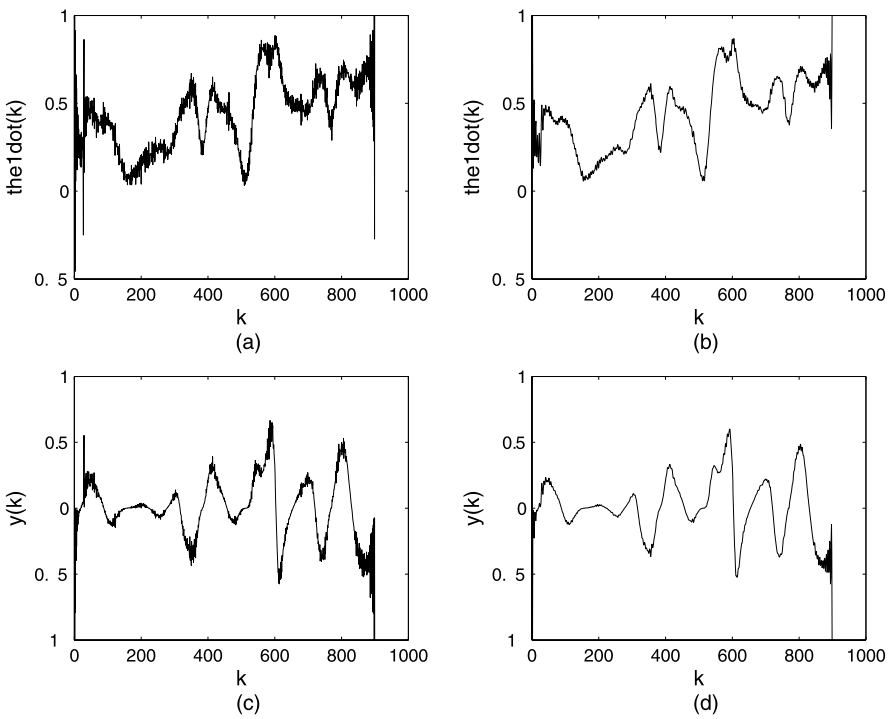

Fig. 7 Signals without and with low-pass filter applied; (**a**) and (**b**) are $\dot{\theta}_1$ without and with filter; (**c**) and (**d**) are y without and with filter applied to each convolution components; k is the kth sampled point of the orbit

Listed in Table 6 are the identified parameters. B_{21} displays a larger error because of the strong nonlinearity of the related term and the relatively larger noise contamination level (due to θ_1's small oscillation amplitude and sensitivity of optical encoders).

5.5 Digital differentiation and error reduction

5.5.1 Recurrence tolerance

Due to the limited length of the experimental data, not many periodic orbits were extracted by setting a small extraction error tolerance, e.g., less than 5% in the present experiment. Thus, one would naturally tend to increase the error tolerance such that more periodic orbits can be extracted. However, with the increased error tolerance and hence more plentiful, but less accurate, periodic orbits, the identification results turned out to get worse for the double pendulum system. Figure 8(a) and (b) display the calculated angular velocity and acceleration curves of a period-9 (Fig. 4) orbit by means of Fourier series expansion method. Obviously, at the location of the recurrence error ($k \approx 800$ as shown in the figure), a large impulse noise generated due to the recurrence error (see Sect. 3.2.3). The noise contamination is even worse for the acceleration signal.

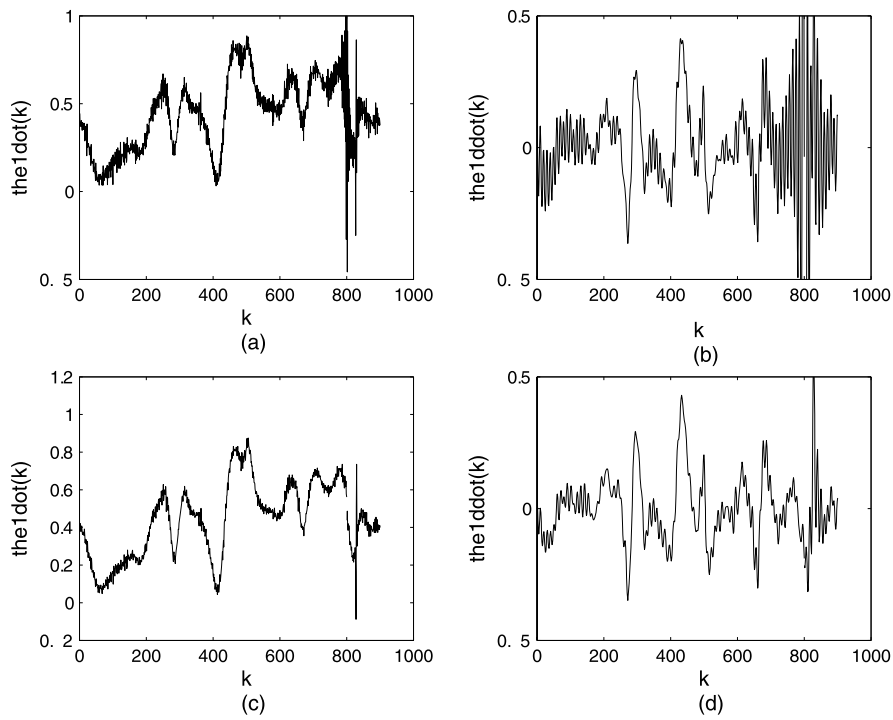

Fig. 8 $\dot{\theta}_1$ and $\ddot{\theta}_1$ orbits obtained by the Fourier Series method (**a**) and (**b**), and by the digital differentiation method (**c**) and (**d**); the recurrence impulses occur at $k = 800$ in (**a**) and (**b**); k is the kth sampled point in the orbit

Table 6 Optimized identification with no digital filter and other methods same as Table 3

Parameters	ID values	True values	Error
B_{11}	0.1125	0.1131	0.5%
B_{12}	0.0790	0.0711	11.1%
B_{15}	0.0825	0.0820	0.6%
B_{21}	1.1611	1.6816	31.0%
B_{22}	0.2553	0.2630	3.0%
B_{25}	0.2564	0.2913	12.0%
C_{11}	0.0003	1.02×10^{-3}	–
C_{12}	−0.0002	0.00366	–
C_2	0.0164	0.0485	–

Table 7 Comparison of calculated values by Fourier Series (FS) method and Digital Differentiation (DD) method when error tolerance is set as 8% and other methods same as Table 3

	FS ID	FS error	DD ID	DD error
B_{11}	0.0126	88.5%	0.1224	8.2%
B_{12}	0.0730	2.7%	0.0760	6.9%
B_{15}	0.0908	10.7%	0.0908	10.7%
B_{21}	1.4703	12.6%	1.6103	4.3%
B_{22}	0.2607	0.9%	0.2559	3.7%
B_{25}	0.2851	2.1%	0.2772	4.8%
C_{11}	0.0014	–	−0.0003	–
C_{12}	0.0005	–	0.0016	–
C_2	0.0053	–	0.0093	–

Table 7 lists the identified parameters (Fourier series method) with 8% error tolerance of extraction (in this case, 58 different orbits extracted), and showed large errors. For the present system, the coefficients B_{11} and B_{21} are parameters of strong nonlinear terms, and therefore identification of these two parameters are usually less stable and more prone to error.

5.5.2 Digital differentiation

Through the previous analysis, for large recurrence error one would naturally consider that a similar scenario would happen to other dynamic systems with strong nonlinearity. In this case, digital differentiation could be applied given adequate sampling points per cycle, e.g., a high sampling rate f_s. In this experiment, there were 100 points per excitation period.

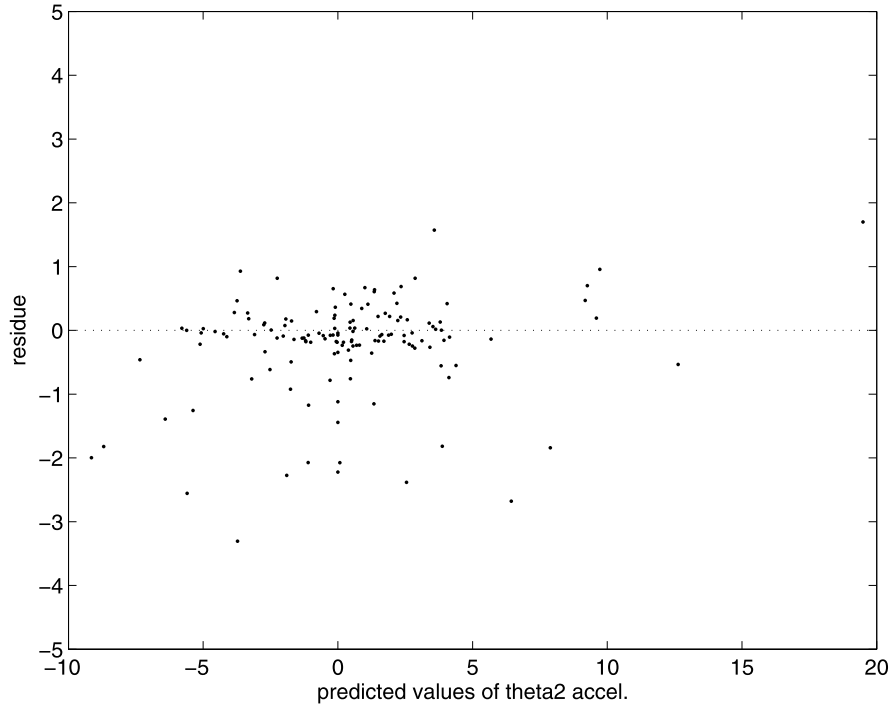

Fig. 9 Identification residue of $\vec{e}_2$ with each dot representing a subharmonic; the horizontal position of each dot is the predicted value of $\vec{q}_2$, the vertical position of each point is the identification residue

The obtained curves are in Fig. 8(c) and (d) for the extracted period-9 orbit. It is apparent that the recurrence impulses are reduced for both of the cases, and much less high frequency noise displayed in the speed and acceleration curves. The corresponding identified parameters listed in Table 7, are more precise compared to those of Fourier series method.

However, the algorithm of digital differentiation itself introduces calculation errors in (16) and (17). It could not predict precisely the small value parameters, e.g., friction parameters, according to an identification test based on the simulated double pendulum system. On the other hand, for the same simulated system, the Fourier series method can identify all of the parameters with satisfying accuracy if the error tolerance of extraction is small enough (2% in this case). It shows that the digital differentiation method is more stable, but not more accurate, compared to the Fourier series expansion algorithm.

5.5.3 Choice of subharmonics or harmonics

Next, we address the optimization strategy of Sect. 3.2.4 for selecting harmonics. Figure 9 displays the residue $\vec{e}_2$ and the corresponding identification error ε_2 is 18.4% when all 140 subharmonics were included in the identification, whose frequencies were less than or equal to the driving frequency. Apparently, the results for B_{2j} for $j = 1, 2, 5$, are not satisfying, and the comparison in Table 8 and Table 3 also corroborates the rule of thumb since B_{21} has a 11.2% error. On the other hand, The B_{1j} parameters have $\varepsilon_1 = 8.8\%$, and are quite consistent with the result after optimization in Table 3.

Table 8 Identified parameters with no optimization to subharmonics set

Parameters	Identified	True values	Error×100%
B_{11}	0.1178	0.1131	4.2%
B_{12}	0.0782	0.0711	10.0%
B_{15}	0.0861	0.0820	5.0%
B_{21}	1.4935	1.6816	11.2%
B_{22}	0.2562	0.2630	0.5%
B_{25}	0.2828	0.2913	3.4%
C_{11}	0.0001	1.02×10^{-3}	–
C_{12}	0.0007	0.00366	–
C_2	0.0147	0.0485	–

For the investigated system, applying the optimization process in Sect. 3.2.4 and after 3 optimization iterations with $\beta = 5\%$ (by excluding 10 erroneous

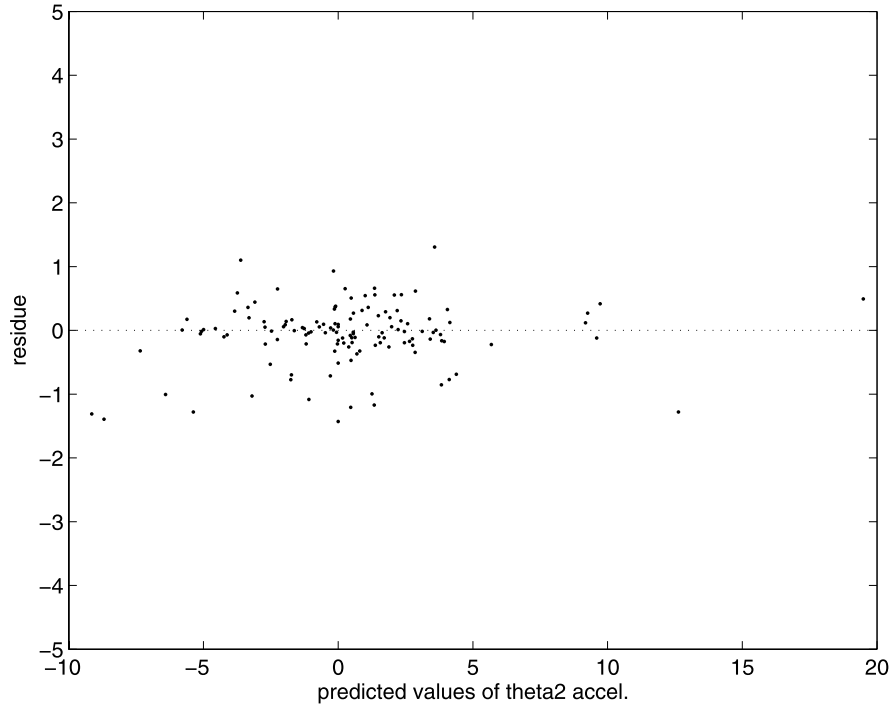

Fig. 10 Identification residue after optimization for $\vec{e}_2$ with each dot representing a subharmonic

subharmonics), the identification errors are reduced to $\varepsilon_1 = 8.1\%$ and $\varepsilon_2 = 9.4\%$. The corresponding results are listed in Table 3. Displayed in Fig. 10 is the residue distribution of $\vec{e}_2$ after optimization. Compared to the identified values without optimization in Table 8, the optimized ones have smaller errors and are more accurate. However, the proposed optimization cannot work well for all cases. If after a few times of optimization the identification errors are still undesirable, we should either use more precise UPOs, or reselect the set of subharmonics before optimization such that the noise contamination can be minimized. In order to obtain more precise UPOs, besides the UPO extraction with smaller tolerance of error, we can also refine the extracted UPOs [22]. But the refinement process may generate erroneous results from quasi-periodic orbits and may not be adequate for limited data set. For better selection of subharmonics, one may choose only those subharmonics that have the largest amplitude in the UPOs' acceleration FFT spectrum (and avoid those noise-contaminated high frequency subharmonics, since it could only be noise). Furthermore, the selection could be simplified by choosing the harmonics instead of subharmonics if most of the orbits are composed mainly of the harmonics of the driving frequency f_e.

5.6 Validation methods

Generally, most of the parameters of a nonlinear system are unknown to us. The direct comparison discussed in previous sections is not available for most applications. Besides, lots of the 'true' parameters in Table 1 were also estimated. Hence, we are not clear what the exact errors are for the identified values. Two other methods were applied here to verify the identified parameters and the effectiveness of the identification algorithm. The first one was to verify our method by identifying the simulated double pendulum system such that comparisons were made based on identification results and the phase portraits of the experimental and simulated systems. The second method involved the linearized system properties, e.g., natural frequencies.

5.6.1 Identification of the simulated double pendulum system

To verify the effectiveness of identification process, a simulated system was also examined with parameters set as the identified values listed in Table 3 except for the friction terms (see Sect. 5.3). The error tolerance of extracting unstable periodic orbits was 5%. The phase

Table 9 Comparison of the identified values and the true parametric settings of the simulated system (methods same as Table 3)

	Identified	Settings	Error×100%
J_{o1} (kg m^2)	5.767×10^{-4}	5.757×10^{-4}	0.2%
J_{o2} (kg m^2)	4.310×10^{-5}	4.228×10^{-5}	1.0%
B_{11}	0.1166	0.1167	0.1%
B_{12}	0.0787	0.0781	0.8%
B_{15}	0.0848	0.0849	0.1%
C_{11}	0.0005	0.0	–
C_{12}	0.0038	0.00366	3.8%
B_{21}	1.5943	1.6149	1.3%
B_{22}	0.2568	0.2562	0.2%
B_{25}	0.2866	0.2868	0.1%
C_2	0.0429	0.0485	11.5%

portrait has been shown in Fig. 5. Some similarity observed in the simulated system compared to the experimental phase portrait (displayed in Fig. 3), e.g., chaotic behavior. Many detailed chaotic characteristics were not available due to the inadequate experimental data. However, it turned out that more UPOs could be extracted from the equally large, sampled data of the simulated system, than from the experimental data set. Meanwhile, for the simulated system, the comparison in Table 9 between the identified values and the parameter settings shows that all the parameters including the friction coefficients were identified correctly, which confirms the effectiveness of this algorithm. The friction coefficients, probably due to their much smaller values and the weakness of the least mean square method, were still hard to calculate very accurately, and thus, identified with larger error percentages. With little noise in the simulated data, the error can only come from the recurrence error of the extracted periodic orbits. Also, it confirms the difficulty of identifying small friction parameters in the experiment, since more noise contamination occurred in the experimental data.

5.6.2 *Linear properties*

The linearized pendulum can also be applied to validate the identification results, e.g., by comparing the natural frequencies of the linearized system. Suppose the pendulum has only a small-angle oscillation without excitation. By discarding the higher order terms and neglecting dry friction, (2) can be simplified to

$$\begin{cases} \frac{d^2\phi_1}{d\tau^2} + B_{11}\frac{d^2\phi_2}{d\tau^2} + B_{12}\phi_1 - C_{12}(\dot{\phi}_2 - \dot{\phi}_1) = 0, \\ \frac{d^2\phi_2}{d\tau^2} + B_{21}\frac{d^2\phi_1}{d\tau^2} + B_{22}\phi_1 - C_2(\dot{\phi}_2 - \dot{\phi}_1) = 0. \end{cases} \tag{19}$$

Since our goal is to examine the natural frequencies, by neglecting the damping terms, (19) can be further simplified to the form of

$$\begin{cases} \frac{d^2\phi_1}{d\tau^2} = \frac{-B_{12}}{1-B_{11}B_{21}}\phi_1 + \frac{B_{22}B_{11}}{1-B_{11}B_{21}}\phi_2, \\ \frac{d^2\phi_2}{d\tau^2} = \frac{B_{12}B_{21}}{1-B_{11}B_{21}}\phi_1 + \frac{-B_{22}}{1-B_{11}B_{21}}\phi_2, \end{cases} \tag{20}$$

and the characteristic matrix of (20) is

$$A = \begin{pmatrix} 0 & 1 & 0 & 0 \\ \frac{-B_{12}}{1-B_{11}B_{21}} & 0 & \frac{B_{22}B_{11}}{1-B_{11}B_{21}} & 0 \\ 0 & 0 & 0 & 1 \\ \frac{B_{12}B_{21}}{1-B_{11}B_{21}} & 0 & \frac{-B_{22}}{1-B_{11}B_{21}} & 0 \end{pmatrix}. \tag{21}$$

The eigenvalues of matrix A are the natural frequencies of the linearized system in nondimensional form. The natural frequencies of the identified system were solved to be 1.336 Hz and 2.904 Hz. Through FFT analysis, the natural frequencies obtained by experimental data are 1.25 Hz and 3.00 Hz. Comparison in Table 10 shows that the natural frequencies match with the FFT result. It shows that the identified parameters excluding the friction terms are reliable for the purpose of system linearization.

Table 10 Natural frequencies

	Identified	Experimental	Error×100%
f_{n1}	1.336	1.25	6.9%
f_{n2}	2.904	3.00	3.2%

6 Conclusions

A double pendulum system experiment was examined for chaotic system identification. The investigated system was a multi-degree-of-freedom system with strong non-linearity, including mixed ϕ_i, $\dot{\phi}_i$ and $\ddot{\phi}_i$ nonlinearity. However, only displacement signals were directly measured data. To adapt to these new challenges, some modifications were added in the harmonic balance identification algorithm:

1. The identification appeared to be less noise-resistant in this case, mainly due to the strong nonlinear term of $(\frac{d\phi_i}{d\tau})^2 \sin(\phi_2 - \phi_1)$ and $\phi_i'' \cos(\phi_2 - \phi_1)$. The high frequency noise contamination in the strong nonlinear terms was reduced with low pass filtering of each component before convolution.

2. Digital differentiation was applied to the experimental data in order to make the identification results more robust even with large recurrence errors in the extracted orbits. It could be of use for limited data sets. However, the digital differentiation algorithm also introduced differentiation error, and thus, did not give accurate values of friction terms.

3. Choices of harmonics also influenced the identified parameters. Inappropriate selection of harmonics can generate poor results. To avoid poor results, the key factor was to avoid noise contaminated harmonics. For the present system, the subharmonics were selected to avoid noise.

4. Linear regression techniques were applied to quantify the identification error ϵ_i, which reflected the error of the identified parameters by examining the residues and the predicted values. Based upon the identification error, an optimization algorithm was proposed to improve the result. An identification error less than 10% indicated a rather satisfying result. However, optimization is limited by statistics, and cannot work for all data to satisfy the rule of thumb.

Friction was a problem in the identification process. For lightly damped systems, since the friction factors were much smaller than other parameters, the identification could not produce accurate values of the friction terms. Noise and recurrence error were the two factors that contributed to this error. However, the harmonic balance algorithm is robust, and the validation process showed that the friction error had little effect on other identified parameters. Meanwhile, the convergence of the identification algorithm was not fully discussed in the experimental study, mainly due to the direct comparison between the identified and the measured parameters. In lieu of convergence, the model was verified using residuals, comparisons to known parameters and linearized properties.

Through the experiment, it can be concluded that the examined identification method can be applied to systems of chaotic, strong nonlinearity and multi-degrees of freedom. With adequate modification, the identification result can be improved, and the quality of the result can be quantified by the identification error.

Acknowledgements We would like to express our appreciation to NASA (grant number NAG-1-01048, with Dr. Walt Silva) and the National Science Foundation (CMS-0099603) for supporting this research. The opinions, findings and conclusions or recommendations expressed in this material are those of the authors and do not necessarily reflect the views of the NASA or NSF.

References

1. Nayfeh, A.H.: Parametric identification of nonlinear dynamic systems. Comput. Struct. **20**(1–3), 487–493 (1985)
2. Hajj, M.R., Fung, J., Nayfeh, A.H., Fahey, S.O.: Damping identification using perturbation techniques and higher order spectra. Nonlinear Dyn. **23**(2), 189–203 (1986)
3. Chen, Q., Tomlinson, G.R.: Parametric identification of systems with dry friction and nonlinear stiffness a time series model. J. Vib. Acoust. **118**(2), 252–263 (1996)
4. Kapania, R.K., Park, S.: Parametric identification of nonlinear structure dynamic systems using finite element method. AIAA J. **35**(4), 719–726 (1997)
5. Chatterjee, A., Vyas, N.S.: Nonlinear parameter estimation in rotor-bearing system using Volterra series and method of harmonic probing. ASME J. Vib. Acoust. Trans. **125**(3), 299–306 (2003)
6. Gottlieb, O., Feldman, M.: Application of a Hilbert-transform based algorithm for parameter estimation of a nonlinear ocean system roll model. J. Offshore Mech. Arct. Eng. **119**, 239–243 (1997)
7. Feldman, M.: Nonlinear free vibration identification via the Hilbert transform. J. Sound Vib. **208**(3), 475–489 (1997)
8. Parlitz, U., et al.: Identification of pre-sliding friction dynamics. Chaos **14**(2), 420–430 (2004)
9. Epureanu, B.I., Dowell, E.H.: System identification for the Ott–Grebogi–Yorke controller design. Phys. Rev. E **56**(5), 5327–5331 (1997)
10. Tufillaro, N.B., Abbott, T., Reilly, J.: An Experimental Approach to Nonlinear Dynamics and Chaos. Addison–Wesley, Redwood City (1992)
11. Auerbach, D., Cvitanovic, P., Eckmann, J.P., Gunaratne, G., Procaccia, I.: Exploring chaotic motion through periodic orbits. Phys. Rev. Lett. **58**, 2387–2389 (1987)
12. Lathrop, D.P., Kostelich, E.J.: Characterization of an experimental strange attractor by periodic orbits. Phys. Rev. A **40**, 4028–4031 (1989)
13. Abarbanel, H.D.I., Brown, R., Sidorowich, J.J., Tsimring, L.S.: The analysis of observed chaotic data in physical systems. Rev. Mod. Phys. **65**, 1331–1392 (1993)
14. Yasuda, K., Kawamura, S., Watanabe, K.: Identification of nonlinear multi-degree-of-freedom systems (presentation of an identification technique). JSME Int. J. Ser. III **31**, 8–14 (1998)
15. Yasuda, K., Kawamura, S., Watanabe, K.: Identification of nonlinear multi-degree-of-freedom systems (identification under noisy measurements). JSME Int. J. Ser. III **31**, 302–309 (1998)
16. Plakhtienko, N.P.: Methods of identification of nonlinear mechanical vibrating systems. Int. Appl. Mech. **36**(12), 1565–1594 (2000)

17. Plakhtienko, N.P.: A method of special weight-functions in the problem of parametric identification of mechanical systems. Dokl. Akad. Nauk A **8**, 31–35 (1983)
18. Ghanem, R., Romeo, F.: A wavelet-based approach for modal and parameter identification of nonlinear systems. Int. J. Non-Linear Mech. **36**(5), 835–859 (2001)
19. Yuan, C.M., Feeny, B.F.: Parametric identification of chaotic systems. J. Vib. Control **4**(4), 405–426 (1998)
20. Feeny, B.F., Yuan, C.M., Cusumano, J.P.: Parametric identification of an experimental magneto-elastic oscillator. J. Sound Vib. **247**(5), 785–806 (2001)
21. Liang, Y., Feeny, B.F.: Parametric identification of chaotic systems, Part I: parametric identification of a simulated horizontally excited pendulum. In: ASME International Mechanical Engineering Congress and RD&D Expo. No. 59836 on CD-ROM (2004)
22. Al-Zamel, Z., Feeny, B.F.: Improved estimations of unstable periodic orbits extracted from chaotic sets. In: 2001 ASME Design Engineering Technical Conferences, Proceedings of DET'01 (2001)